J|A|C|S
ARTICLES

Published on Web 06/21/2010

Designing Green Oxidation Catalysts for Purifying Environmental Waters

W. Chadwick Ellis,[†] Camly T. Tran,[†] Riddhi Roy,[†] Marte Rusten,[‡,||] Andreas Fischer,[§] Alexander D. Ryabov,[†] Bruce Blumberg,*[,‡] and Terrence J. Collins*[,†]

Department of Chemistry, Institute of Green Science, Mellon Institute, Carnegie Mellon University, Pittsburgh, Pennsylvania 15213, Department of Developmental and Cell Biology, University of California, Irvine, California, Royal Institute of Technology, Department of Chemistry, Stockholm, Sweden, and Department of Molecular Biology, University of Bergen, Norway

Received March 25, 2010; E-mail: tc1u@andrew.cmu.edu

Abstract: We describe the synthesis, characterization, aqueous behavior, and catalytic activity of a new generation of Fe^{III}−TAML (tetraamido macrocycle ligand) activators of peroxides (**2**), variants of $[Fe\{(OC)_2(o,o'\text{-}NC_6H_4NCO)_2CMe_2\}(OH_2)^-]$ (**2d**), which have been designed to be especially suitable for purifying water of recalcitrant oxidizable pollutants. Activation of H_2O_2 by **2** (k_I) as a function of pH was analyzed via kinetic studies of Orange II bleaching. This was compared with the known behavior of the first generation of Fe^{III}−TAMLs (**1**). Novel reactivity features impact the potential for oxidant activation for water purification by **2d** and its aromatic ring-substituted dinitro (**2e**) and tetrachloro (**2f**) derivatives. Thus, the maximum activity for **2e** occurs at pH 9, the closest yet to the EPA guidelines for drinking water (6.5−8.5), allowing **2e** to rapidly activate H_2O_2 at pH 7.7. In water, **2e** has two axial water ligands with pK_a's of 8.4 and 10.0 (25 °C). The former is the lowest for all Fe^{III}−TAMLs developed to date and is key to **2e**'s exceptional catalytic activity in neutral and slightly basic solutions. Below pH 7, **2d** was found to be quite sensitive to demetalation in phosphate buffers. This was overcome by iterative design to give **2e** (hydrolysis rate **2d** > 100 × **2e**). Mechanistic studies highlight **2e**'s increased stability by establishing that to demetalate **2e** at a comparable rate to which $H_2PO_4^-$ demetalates **2d**, H_3PO_4 is required. A critical criterion for green catalysts for water purification is the avoidance of endocrine disruptors, which can impair aquatic life. Fe^{III}−TAMLs do not alter transcription mediated by mammalian thyroid, androgen, or estrogen hormone receptors, suggesting that **2** do not bind to the receptors and reducing concerns that the catalysts might have endocrine disrupting activity.

Introduction

Everyone needs an adequate supply of clean water to live a healthy life,[1] yet pure water is getting harder to come by as, among other things, contamination by synthetic chemicals increases on a global scale.[2,3] The stakes for health and the environment are compounded by findings that certain everyday chemicals we have long assumed to be safe are endocrine disruptors (EDs) that can interfere with cellular development at environmentally relevant concentrations to impair living things.[4] Fe^{III}−TAMLs (Chart 1) are small-molecule catalysts that activate hydrogen peroxide via peroxidase-like cycles to rapidly and efficiently[5] purify water of many chemicals, including EDs,[6−8] as well as hardy pathogens.[9] The prototype (**1a**, Chart 1) is in commercial use, and others will follow.

Chart 1. Fe^{III}−TAML Activators of Peroxides of the First (**1**) and Second (**2**) Generation Discussed in This Work

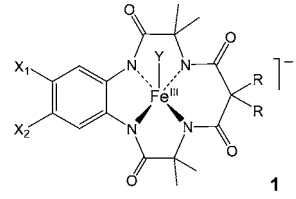

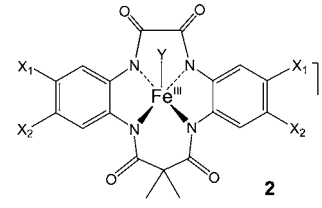

(**a**) $X_1 = X_2 = H$, R = CH_3
(**b**) $X_1 = X_2 = Cl$, R = F
(**c**) $X_1 = NO_2$, $X_2 = H$, R = F
(**d**) $X_1 = X_2 = H$
(**e**) $X_1 = NO_2$, $X_2 = H$
(**f**) $X_1 = X_2 = Cl$

[†] Carnegie Mellon University.
[‡] University of California.
[||] University of Bergen.
[§] Royal Institute of Technology.

(1) *Guidelines for Drinking Water Quality*, 3rd ed.; World Health Organization: Geneva, 2008.
(2) U.S. Geological Survey.Water Quality http://www.usgs.gov/science/science.php?term=1306.
(3) Daughton, C. G. *Compr. Anal. Chem.* **2007**, *50*, 1–58.
(4) Diamanti-Kandarakis, E.; Bourguignon, J.-P.; Giudice, L. C.; Hauser, R.; Prins, G. S.; Soto, A. M.; Zoeller, R. T.; Gore, A. C. *Endocr. Rev.* **2009**, *30*, 293–342.
(5) Ryabov, A. D.; Collins, T. J. *Adv. Inorg. Chem.* **2009**, *61*, 471–521.
(6) Chanda, A.; Khetan, S. K.; Banerjee, D.; Ghosh, A.; Collins, T. J. *J. Am. Chem. Soc.* **2006**, *128*, 12058–12059.
(7) Sen Gupta, S.; Stadler, M.; Noser, C. A.; Ghosh, A.; Steinhoff, B.; Lenoir, D.; Horwitz, C. P.; Schramm, K.-W.; Collins, T. J. *Science* **2002**, *296*, 326–328.

 10.1021/ja102524v

Fe^{III}−TAML catalysis rates are significantly pH dependent, maximizing for generation **1** (the B* series) in the 10−11 range.[5,10,11] This presents the intriguing design challenge of achieving the maximum rate in the 5−8 pH range commonly found for natural waters.[12] Environmental performance also can be advanced by improving the resistance of Fe^{III}−TAML to degradation by protic ligands (general acids)[13] that are often present in polluted waters and by removing concerns in a precautionary sense that Fe^{III}−TAML technologies might contaminate water with persistent catalyst degradation fragments. With regard to this last design target, until recently only the most aggressive first generation Fe^{III}−TAML would rapidly oxidize persistent pollutants—all were fluorinated and one was additionally chlorinated.[10,11] To escape the prospect of fluoride or persistent organohalogen residues arising from Fe^{III}−TAML processes, generation **2** catalysts were successfully designed to achieve high reactivity and to be able to be highly reactive and fluorine- and chlorine-free for commercially viable catalysts,[14] but it has turned out that the catalysts **2** deliver other significant performance advantages for environmental applications.

On the basis of equilibrium and kinetic data, we explain here the structure−activity factors that give **2e** a maximum activity closer to neutral pH than any prior Fe^{III}−TAML and why it is much more resistant than **2d** to demetalation by common, protic, water-borne ligands. From this understanding of the etiology of **2e**'s superior properties, Fe^{III}−TAML design is set up to achieve even higher performance and more environmentally beneficial homogeneous oxidation catalysts. At the scientific level, iron−TAML compounds represent the best available catalytic solution to the oxidative purification of large quantities of water. Many other oxidation catalysts exist, but their applications require nonaqueous conditions or they achieve few turnovers.[15−17]

Experimental Section

Materials and Methods. Kinetic measurements were carried out using Hewlett-Packard diode array spectrophotometers (models 8452A and 8453) equipped with a thermostated cell holder and automatic 8-cell positioner using plastic poly(methyl methacrylate) 1 cm cuvettes. Measurements of the UV/vis spectra of **2e** for determining its pK_a values were carried out on a Cary 5000 UV/vis-NIR spectrophotometer (Varian) in quartz cells. ^{1}H NMR data were collected at 300 K with a Bruker Avance 300 instrument operating at 300 MHz in DMSO-d_6, the chemical shifts (δ) being referenced to the residual proton DMSO signal at δ 2.5. Combustion analyses were performed by Midwest Microlabs, LLC. Bioluminescence assays were performed using a Dynatech ML3000 microplate luminometer, and colorimetric β-galactosidase assays were performed using a Molecular Devices Spectramax plate reader. The Fe^{III}−TAML **2e** was synthesized as indicated previously.[14] All reagents and solvents were at least ACS reagent grade in quality and were obtained from commercial sources. They were used as received or, if noted, after purification as described elsewhere.[18] Orange II was purified by column chromatography on reversed-phase silica gel using SMT-Bulk C18 no. BOD-35-150 resin (Separation Methods Technologies) using water as an eluent.

Synthesis of 2d (Scheme 1S, Supporting Information). 1,2-Diaminobenzene (9 g, 0.083 mol) was dissolved in freshly distilled THF (100 mL), and triethylamine (15 mL) was added. Di-*tert*-butyl dicarbonate (Boc_2O) (18 g, 0.082 mol) was dissolved in THF (50 mL) and placed in a dropping funnel. The solution was added dropwise to the 1,2-diaminobenzene solution with rapid stirring and was then stirred overnight. The THF was removed by the rotary evaporation to yield a yellow viscous residue, which yielded yellow-brown crystals in the freezer (−25 °C). The crystals were separated and recrystallized from hot ethanol to yield (2-aminophenyl)carbamic acid 1,1-dimethylethyl ester (**A**; 10.5 g, 61%). ^{1}H NMR (DMSO-d_6): 1.45 (s, 9H, ^{t}Bu), 4.8 (s, 2H, NH_2), 6.55 (td, 1H, ArH), 6.7(dd, 1H, ArH), 6.85(td, 1H, ArH), 7.2 (dd, 1H, ArH), 9.65 (br s, 1H, CONHBoc). Anal. Calcd for $C_{11}H_{16}N_2O_4$ (208.26): C, 63.44; H, 7.74; N, 13.45. Found: C, 63.53; H, 7.7; N, 13.7. Compound **A** (4 g, 0.0192 mol) was dissolved in dry THF (100 mL), and pyridine (2 mL) was added. Dimethylmalonyl dichloride (1.31 mL, 0.00958 mol) dissolved in dry THF (50 mL) was added at a rate of 1 drop every 3 s using a dropping funnel. A white precipitate of pyridinium chloride formed and was removed by filtration. Removal of THF from the filtrate under vacuum gave a viscous oil, which was placed in the freezer (−25 °C) to form a precipitate which was further purified by sonication in hexane for 10 min. Solid 2-[[3-[[2-[[(1,1-dimethylethoxy)carbonyl]amino]phenyl]amino]-2,2-dimethyl-1,3-dioxopropyl]amino]phenyl]carbamic acid 1,1-dimethylethyl ester (**B**) was collected by filtration in greater than 90% yield. ^{1}H NMR (DMSO-d_6): 1.4 (s, 18H, ^{t}Bu), 1.55 (s, 6H, CH_3), 7.15 (m, 4H, ArH), 7.5 (m, 4H, ArH), 8.7 (s, 2H, CONH), 9.3 (s, 2H, CONH). Aqueous 12 N HCl (45 mL) was added slowly to solution of **B** (2.5 g, 0.0049 mol) in ethyl acetate (150 mL) with rapid mixing. After being stirred for 5 min, the mixture was quenched with aqueous NaOH (20 g in 500 mL) in an ice bath with rapid stirring. The pH of the aqueous layer was raised to 11 with NaOH, and the organic and aqueous layers were separated. The aqueous layer was extracted three times with CH_2Cl_2 (100 mL each). All organic layers were combined, dried over $MgSO_4$, and filtered. The volume was reduced to 4 mL, and the residue was sonicated in diethyl ether (15 mL) to afford solid N^1,N^3-bis(2-aminophenyl)-2,2-dimethylpropanediamide (**C**; 1.12 g, 74%). ^{1}H NMR (DMSO-d_6): 1.55 (s, 6H, CH_3), 4.9 (br s, 4, NH_2), 6.55 (m, 2H, ArH), 6.73 (m, 2H, ArH), 6.97 (m, 2H, ArH), 9.0 (s, 2H, CONH). Anal. Calcd for $C_{17}H_{20}N_4O_2$ (312.37): C, 65.37; H, 6.45; N, 17.94. Found: C, 64.95; H, 6.36; N, 17.8%. Compound **C** (128 mg, 0.410 mmol) was dissolved in dry THF (50 mL) and NEt_3 (0.115 mL, 0.903 mmol). Oxalyl chloride (0.205 mL of 2 M solution in CH_2Cl_2; 0.410 mmol) in dry THF (30 mL) was added overnight at a rate of 1 drop each 5 s using a dropping funnel with stirring. A precipitate formed over 12 h. After addition of CH_2Cl_2 (125 mL), the mixture was treated with 0.1 M $KHSO_4$ (100 mL), 0.1 M $NaHCO_3$ (100 mL), and H_2O (100 mL) in a separation funnel. A white solid in the organic phase was filtered through a sintered glass crucible and washed with diethyl ether (5 mL) and petroleum ether (5 mL) to give a first crop of the macrocycle, 15,15-dimethyl-5,8,13,17-tetrahydro-

(8) Shappell, N. W.; Vrabel, M. A.; Madsen, P. J.; Harrington, G.; Billey, L. O.; Hakk, H.; Larsen, G. L.; Beach, E. S.; Horwitz, C. P.; Ro, K.; Hunt, P. G.; Collins, T. J. *Environ. Sci. Technol.* **2008**, *42*, 1296–1300.
(9) Banerjee, D.; Markley, A. L.; Yano, T.; Ghosh, A.; Berget, P. B.; Minkley, E. G., Jr.; Khetan, S. K.; Collins, T. J. *Angew. Chem., Int. Ed.* **2006**, *45*, 3974–3977.
(10) Ghosh, A.; Mitchell, D. A.; Chanda, A.; Ryabov, A. D.; Popescu, D. L.; Upham, E.; Collins, G. J.; Collins, T. J. *J. Am. Chem. Soc.* **2008**, *130*, 15116–15126.
(11) Popescu, D.-L.; Chanda, A.; Stadler, M. J.; Mondal, S.; Tehranchi, J.; Ryabov, A. D.; Collins, T. J. *J. Am. Chem. Soc.* **2008**, *130*, 12260–12261.
(12) EPA website: http://www.epa.gov/safewater/consumer/2ndstandards.html.
(13) Polshin, V.; Popescu, D.-L.; Fischer, A.; Chanda, A.; Horner, D. C.; Beach, E. S.; Henry, J.; Qian, Y.-L.; Horwitz, C. P.; Lente, G.; Fabian, I.; Münck, E.; Bominaar, E. L.; Ryabov, A. D.; Collins, T. J. *J. Am. Chem. Soc.* **2008**, *130*, 4497–4506.
(14) Ellis, W. C.; Tran, C. T.; Denardo, M. A.; Fischer, A.; Ryabov, A. D.; Collins, T. J. *J. Am. Chem. Soc.* **2009**, *131*, 18052–18053.
(15) Meunier, B. *Biomimetic Oxidations Catalyzed by Transition Metal Complexes*; Imperial College Press: London, 2000.
(16) Meunier, B. *Models of Heme Peroxidases and Catalases*; Imperial College Press: London, 2000.
(17) Marques, H. M. *Dalton Trans.* **2007**, 4371–4385.
(18) Perrin, D. D.; Armarego, W. L. F. *Purification of Laboratory Chemicals*, 3rd ed.; Pergamon Press: Oxford, 1988.

5,8,13,17-tetraazadibenzo[*a*,*g*]cyclotridecene −6,7,14,16-tetraone (**D**; 41 mg, 25%). The filtrate was dried over $MgSO_4$, and the volume was reduced to ca. 3 mL. A precipitate formed upon trituration with petroleum ether, which was filtered to yield a second crop of **D** (72.5 mg, 44%). ^{1}H NMR (DMSO-d_6): 9.65 (s, 2H, CONH$^{\alpha}$), 9.55 (s, 2H, CONH$^{\beta}$), 7.625 (m, 2H, ArH), 7.35 (m, 6H, ArH), 1.56 (s, 6H, CH_3). Anal. Calcd for $C_{19}H_{18}N_4O_4$ (366.37): C, 62.3; H, 4.95; N, 15.29. Found: C, 61.83; H, 5.12; N, 14.51. Metalation of **D** to yield **2d** was performed as previously described.[14] ESI-MS (negative mode) for PPh_4[**2d**(H_2O)]: 418.1 *m*/*z*; isotopic peaks 419.09 (23%), 416.17 (4%) *m*/*z*.

Synthesis of 2f. The corresponding sodium salt was prepared using a slightly modified procedure compared to that employed for **2e**.[14] Removal of Boc from *N*,*N*′-bis(2-carbamic acid *tert*-butyl ester-4,5-dichlorophenyl)-2,2-dimethylmalonamide to yield *N*,*N*′-bis(2-amino-4,5-dichlorophenyl)-2,2-dimethylmalonamide was performed in acetic acid (instead of ethyl acetate as with **2e**) using 3 M HCl. The macrocyclic precursor was isolated by precipitation as the dihydrochloride salt using ice-cold diethyl ether. The macrocyclization and metalation steps were performed as described for **2e**. The sodium cation was metathetically exchanged with the bis(triphenylphosphoranylidene)ammonium ([PNP^+]) cation. The salt Na[**2f**] (4 mg) was dissolved in water (2 mL) and mixed dropwise with excess [PNP]Cl (ca. 80 mg dissolved in 4 mL of a 1/1 v/v MeOH/H_2O) with stirring. The reddish orange precipitate was collected by filtration and was recrystallized from MeOH/H_2O. X-ray quality crystals of [PNP]**2f** (Y = H_2O) were obtained by slow evaporation of methanol from water. Anal. Calcd for [PNP]**2f**·(H_2O)$_3$, $C_{55}H_{46}Cl_4FeN_5O_7P_2$ (1148.59): C, 57.51; H, 4.04; N, 6.10. Found: C, 57.04; H, 3.84; N, 5.93.

Demetalation of 2. Compound **2d** (20 mg) was dissolved in phosphate buffer (2 mL, 0.5 M, pH 8). The solution was kept overnight at 22 °C. Colorless needlelike crystals formed which were contaminated by an amorphous brown precipitate. These were separated manually, washed with water, and air dried. The ^{1}H NMR data (δ, DMSO-d_6) confirmed the material to be the macrocyclic ligand expected from hydrolysis of **2d**: 9.65s, 2H (NH); 9.55s, 2H (NH), 7.7−7.2, m, 8H (ArH), 1.56s, 6H (CH_3).

Kinetic Measurements. (A) Demetalation. The kinetics of demetalation of **2d**,**e** was measured at phosphate concentrations 0.1, 0.3, and 0.5 M at 25 °C as described previously.[13] A stock solution of **2d** in MeCN (0.005 M) was added to the phosphate buffer in a 1 cm plastic cuvette to give a [**2d**] of ca. 4.5×10^{-5} M, and changes in absorbance were recorded at 350 nm. Measurements were performed in the pH range of 4.0−9.5. Pseudo-first-order rate constants (k_{obs}) were calculated by fitting the absorbance (A) versus time (t) traces to the equation $A = A_\infty - (A_\infty - A_0) \times \exp(-k_{obs}t)$ where A_0 and A_∞ are absorbances at $t = 0$ and ∞, respectively. Satisfactory first-order kinetics holds for at least 4−5 half-lives. The rate constants k_{obs}, which are mean values of at least three determinations, were plotted against total phosphate concentration to obtain $k_{1,eff}$ as the slope of the linear plot. Measurements for **2e** were performed at 385 nm as described for **2d**, but the pH range of 1−5 was also covered. Calculations were performed using a Sigma Plot 2007 package (version 10.0) or Mathematica 7.0. **(B) Bleaching of Orange II.** Initial rates of bleaching of Orange II by H_2O_2 catalyzed by **2** were measured essentially as described in detail previously[19] in the range of H_2O_2 concentrations 0.0003−0.0015 M at an [Orange II] of 4×10^{-5} M. Solutions of H_2O_2 were standardized daily by measuring the absorbance at 230 nm (ε = 72.8 M^{-1} cm^{-1}).[20] In this work, extinction coefficients (ε) of Orange II were measured at each pH used in the kinetic experiments giving values of 19000 M^{-1} cm^{-1} at pH 6.0−10.0 and 17700, 15500, 14100, and 11500 M^{-1} cm^{-1} at pH 10.5, 11.0, 11.5, and 12.0, respectively. **(C) Comparative Bleaching of Orange II at pH 7.7.** A 1.5 mL aliquot of a stock solution of Orange II (4.9×10^{-5} M) in 0.01 M phosphate buffer added was added to a cuvette. Stock solutions of [PPh_4]**2d**, [PPh_4]**2e**, and [PNP]**2f** were made in acetonitrile, and approximately 10 μL was added into the cuvette to make the concentration of iron of 2×10^{-7} M. An aliquot of H_2O_2 was added such that the concentration in the cuvette was 4.4×10^{-4} M. The absorbance of Orange II was monitored at 485 nm.

X-ray Crystallography Details for 2f: $C_{55}H_{42}Cl_4FeN_5O_6P_2$; M_r = 1128.6, crystal dimensions 0.20 × 0.29 × 0.37 mm^3, triclinic, *P*-1, *a* = 10.7084(9) Å, *b* = 16.545(2) Å, *c* = 16.912(2) Å, α = 116.991(8)°, β = 99.824(9)°, γ = 94.007(9)°, *V* = 2593.5(5) $Å^3$, *Z* = 2, ρ_{calc} = 1.445 Mg·m^{-3}, μ = 0.62 mm^{-1}, Mo Kα, λ = 0.71073 Å, *T* = 299 K, $2\theta_{max}$ = 55°, 55 025 measured reflections, 11780 independent reflections, R_{int} = 0.045, *R* = 0.046 (7777 observed reflections), wR_2 = 0.114, *S* = 1.04, residual electron density 0.70/−0.54. Refinement on F^2 with anisotropic displacement parameters for all non-H atoms.

Luciferase Reporter Assays of Receptor Activation. COS7 cells were cultured in phenol-red-free Dulbecco's modified Eagle medium (DMEM) supplemented with 10% bovine calf serum. Twenty-four hours before transfection, the cells were seeded at a density of 5×10^5 cells per 96-well plate. Plasmids expressing either the full-length receptors (AR, ERα), or a chimeric protein where the ligand binding domain of the receptor is fused to the DNA binding domain of GAL4 (TRβ), were cotransfected with their respective reporter constructs and pCMX-β-galactosidase control plasmid using calcium-phosphate mediated transfection as previously described.[21] The expression plasmids and their reporter constructs have been described elsewhere.[22] The test compounds were initially dissolved in doubly distilled water (Fe^{III}−TAML) or DMSO (control ligands), and subsequently diluted in DMEM supplemented with 10% charcoal-resin stripped fetal bovine serum (FBS) to a final solvent concentration of 0.5%. After 24 h of ligand exposure, 50 μL aliquots of cell lysates were assayed for luciferase and β-galactosidase activity by standard protocols.[22] Luciferase activity was normalized to β-galactosidase activity to control for transfection efficiency and reported as fold activation relative to the vehicle control.

Results and Discussion

Synthesis, Characterization, and Prescreening of Catalytic Activity of D* TAML Catalysts 2. Usually, Fe^{III}−TAML activators of peroxides substituted with electron-withdrawing chloro and nitro groups show advantageous reactivity (higher oxidative reactivity and hydrolytic stability) compared with similar catalysts with electron-donating fragments.[5] This explains why Fe^{III}−TAMLs **2d**−**f** were chosen for synthesis and comparative evaluation. The preparation of the tetrachlorinated catalyst **2f** was carried out similarly to **2e**.[14] A minor variation involved using HCl in acetic acid as a medium for deprotection of the macrocyclic precursor, which was isolated as a diamine dihydrochloride salt. The study of **2f** by X-ray crystallography revealed a square pyramidal geometry, which is typical of these small molecule peroxidase replicas (Figure 1).[5] A new hydrogen bond system found in the structure of **2f** is noteworthy. The axial water ligand of a first Fe^{III}−TAML anion forms two hydrogen bonds with amide oxygens of the second Fe^{III}−TAML anion, the aqueous ligand of which, in turn, forms two H-bonds with the first Fe^{III}−TAML anion. Thus, four H···O interactions produce a dimeric motif in the solid state structure of **2f**.

Orange II is a convenient dye for preliminary screening of Fe^{III}−TAML/H_2O_2 catalysis. It has been successfully used by

(19) Chahbane, N.; Popescu, D.-L.; Mitchell, D. A.; Chanda, A.; Lenoir, D.; Ryabov, A. D.; Schramm, K.-W.; Collins, T. J. *Green Chem.* **2007**, *9*, 49–57.
(20) George, P. *Biochem. J.* **1953**, *54*, 267–276.
(21) Grun, F.; Venkatesan, R. N.; Tabb, M. M.; Zhou, C.; Cao, J.; Hemmati, D.; Blumberg, B. *J. Biol. Chem.* **2002**, *277*, 43691–43697.
(22) Blumberg, B.; Sabbagh, W., Jr.; Juguilon, H.; Bolado, J., Jr.; Van Meter, C. M.; Ong, E. S.; Evans, R. M. *Genes Dev.* **1998**, *12*, 3195–3205.

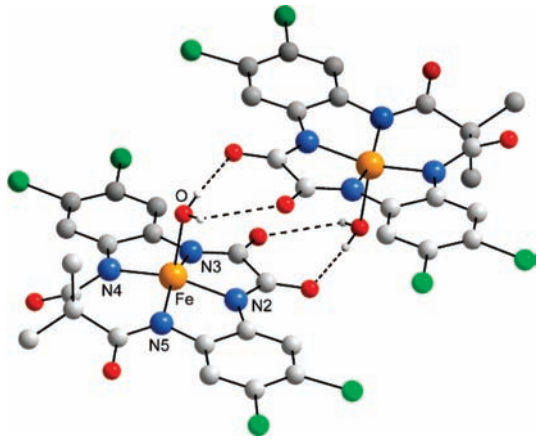

Figure 1. ORTEP diagram of the anionic part of [PNP]**2f** with Y = water (Fe in yellow, O in red, N in blue, and Cl in green; only H atoms of the aqua ligand are shown for clarity). The Fe−N bond distances equal 1.8701(23), 1.8637(22), 1.8943(20), and 1.8912(25) Å; the Fe−O bond distance is 2.1102(18) Å.

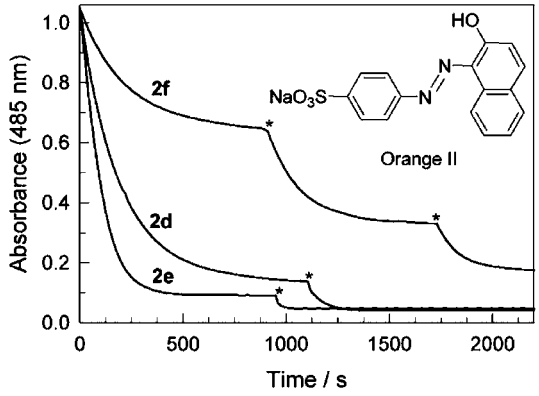

Figure 2. Bleaching of Orange II (4.9×10^{-5} M) by H_2O_2 (4.4×10^{-4} M) catalyzed by complexes **2d**−**f** (2×10^{-7} M); asterisks indicate points of addition of a new aliquot of **2** (2×10^{-7} M). Conditions: pH 7.7, 0.01 M phosphate, 25 °C.

us[5] and by other researchers as an easy-to-follow substrate in catalyzed oxidation reactions.[23,24] The data in Figure 2 compare the catalytic performance of **2d**−**f** at neutral pH using aliquots of **2** (each time to return the solution to the 200 nM starting concentration) with >200 molar equiv of Orange II. As can be seen, a single aliquot of the dinitro-substituted catalyst **2e** caused the fastest and the deepest bleaching. More than 90% of Orange II was degraded in less than 500 s. The catalyst **2d** is slightly less aggressive under the same conditions. The catalytic performance of the tetrachloro derivative **2f** is significantly less in terms of both the speed and conversion. One aliquot of the catalyst destroyed less than 40% of the dye. The bleaching was still incomplete after adding two more aliquots of **2f**. This screening revealed the superiority in bleaching of **2d** and **2e**.

Demetalation by General Acids: Remarkable Changeover. The stability of **1a** in aqueous solution is decreased in the presence of proton donors, e.g., $H_2PO_4^-$, HSO_4^-, and HCO_3^-—a mechanism for the hydrolysis process has been proposed.[13] While the rate of iron ejection is orders of magnitude slower

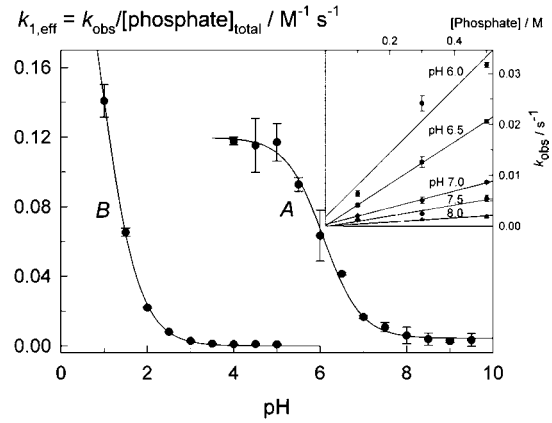

Figure 3. Second-order rate constants $k_{1,eff}$ as a function of pH for the phosphate-induced demetalation of **2d** (*A*) and **2e** (*B*) at 25 °C. Inset: dependence of k_{obs} on total phosphate concentration for demetalation of **2d**.

Scheme 1. Mechanism of the Buffer (General Acid) Promoted "Coordinative" Iron Ejection from Fe^{III}−TAMLs

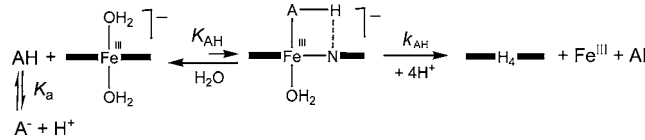

than oxidation catalysis,[10,11,13,25] long-term storage of **1a** in pH ≤ 8 aqueous solutions buffered by such ions is prohibited by this intrinsic property.[13] Moreover, since these ions are often present in environmental waters, there is considerable potential for interruption of trace contaminant purification because, at the ultralow concentrations of catalyst, peroxide, and the targeted contaminants, any catalyst must perform for many hours to be effective. The buffer-ion induced "coordinative" demetalation of **1a** manifests experimentally in linear dependencies of the pseudo-first-order demetalation rate constants k_{obs} on the total phosphate concentration (with the slopes of the linear plots giving the second-order rate constants $k_{1,eff}$). The rate constants $k_{1,eff}$ increase hyperbolically with increasing proton concentration.[13]

The second-generation catalyst, **2d**, exhibits similar behavior. The values of k_{obs} depend linearly on the total phosphate concentration (Inset to Figure 3), whereas the second-order rate constant $k_{1,eff}$ exhibits a sigmoid dependence on pH with the inflection point around 6.5 (Figure 3A). This behavior is fully accountable in terms of the "coordinative" demetalation reaction mechanism (Scheme 1) with the active demetalating species being dihydrogen phosphate, $H_2PO_4^-$, and the rate expression 1 for $k_{1,eff}$ being[13]

$$k_{1,\mathrm{eff}} = \frac{k_\alpha[\mathrm{H}^+]}{K_\mathrm{a} + [\mathrm{H}^+]} \qquad (1)$$

Here, k_α is the second-order rate constant proposed for proton delivery from the demetalating ion (general acid) to an amido nitrogen atom of Fe^{III}−TAML, and K_a is the dissociation constant under discussion.[13] Obviously, k_α is a composite value and equals $K_{AH}k_{AH}$ in terms of the mechanism in Scheme 1

(23) Ember, E.; Rothbart, S.; Puchta, R.; van Eldik, R. *New J. Chem.* **2009**, *33*, 34–49.
(24) Theodoridis, A.; Maigut, J.; Puchta, R.; Kudrik, E. V.; Van Eldik, R. *Inorg. Chem.* **2008**, *47*, 2994–3013.
(25) Chanda, A.; Ryabov, A. D.; Mondal, S.; Alexandrova, L.; Ghosh, A.; Hangun-Balkir, Y.; Horwitz, C. P.; Collins, T. J. *Chem.—Eur. J.* **2006**, *12*, 9336–9345.

Table 1. Kinetic ($k_\alpha = K_{AH}k_{AH}$) and Thermodynamic (pK_a) Parameters of Eq 1 and Scheme 1 Responsible for the Buffer (General Acid) Promoted "Coordinative" Iron Ejection from Fe^{III}−TAMLs

Fe^{III}−TAML	T/°C	AH	$k_\alpha/M^{-1}\ s^{-1}$	$pK_a/(K_\alpha$ in M)	ref
1a	25	$H_2PO_4^-$	1.3×10^{-3a}	6.55	14
2d	25	$H_2PO_4^-$	0.12 ± 0.03	6.12 ± 0.14	this work
2e	40	$H_2PO_4^-$	$(6.3 \pm 1.2) \times 10^{-3b}$	5.5 ± 0.5	
	50	$H_2PO_4^-$	$(1.5 \pm 0.1) \times 10^{-2}$	6.1 ± 0.2	
	60	$H_2PO_4^-$	$(2.0 \pm 0.1) \times 10^{-2}$	5.8 ± 0.1	
	70	$H_2PO_4^-$	$(3.0 \pm 0.2) \times 10^{-2}$	6.1 ± 0.1	
	25	$H_2PO_4^-$	3.0×10^{-3c}		
2e	25	H_3PO_4	0.31 ± 0.01	0.91 ± 0.05	this work

[a] $\Delta H^{\ddagger}$ 47 kJ mol^{-1}, $\Delta S^{\ddagger}$ −143 J K^{-1} mol^{-1}.[14] [b] $\Delta H^{\ddagger}$ 42 ± 7 kJ mol^{-1}, $\Delta S^{\ddagger}$ −150 ± 20 J K^{-1} mol^{-1}. [c] Extrapolated value.

because the equilibrium for ligation by AH is strongly shifted to the left. Fitting the experimental data in Figure 3A to eq 1 gave the values of k_α and pK_α summarized in Table 1. The values for **1a** are included for comparison. It is noteworthy that the rate constant k_α for **2d** is larger than that for **1a**,[13] and therefore, we decided to enhance the stability of the second generation catalysts **2** by introducing the electron-withdrawing nitro substituents as in **2e**. The choice of the nitro groups was dictated by two previously discovered observations−the nitro substituents increase both the catalytic performance[11] and the operational stability (resistance to suicidal inactivation)[25] of Fe^{III}−TAMLs. It might be more reasonable to anticipate that a more powerful oxidant would have a higher tendency for the self-oxidation such that findings are consistent with suicidal inactivation proceeding at the aromatic rings since the nitro groups would locally protect the rings from oxidation even while globally activating the iron reactive intermediates.[25]

The very first measurements with nitro-substituted **2e** indicated its significantly higher resistance to the phosphate-induced demetalation compared to **2d**. The reaction rate was very low at pH 6 and 25 °C. Rates comparable to those of **2d** were observed at markedly lower pH, specifically, below 2.5 where the free proton (specific acid) catalyzed demetalation of Fe^{III}−TAMLs **1** could come into play.[26] Therefore, the H^+- and phosphate-catalyzed pathways for iron ejection were carefully separated for **2** catalysts. This was achieved by plotting k_{obs} vs [total phosphate] at constant pH for a variety of pHs. The slope of the line delivers rate information for the phosphate dependent demetalation. The intercept delivers information on all other demetalating processes, including those brought about by the specific acid (see inset to Figure 3 as an example).[26] Calculation of the $k_{1,eff}$ values for **2e** over pH 1.0 to 5.0 resulted in the pH profile shown in Figure 3B, which clearly shows that dihydrophosphate ($H_2PO_4^-$) is much less reactive toward **2e** and that coordination of the more acidic phosphoric acid (H_3PO_4) is needed for the ejection of iron(III) from the macrocyclic cavity of **2e** at a similar rate to that which $H_2PO_4^-$ produces for **2d**. The data in Figure 3B were also fitted to eq 1, and the best-fit values are included in Table 1. The pK_a value of 0.91 suggests the involvement of trihydrogen phosphate (pK_a 1.70[27]) in the demetalation process.

In order to compare the reactivity of $H_2PO_4^-$ toward **2d** and **2e**, the measurements with **2e** in the pH range of 5.0−7.5 were performed at higher temperatures, viz. 40−70 °C. Equation 1 was found to be operative in all cases, and the corresponding values of k_α and K_a are included in Table 1. The Eyring equation was applied to k_α in this temperature range (Figure 1S, Supporting Information). The values of the activation parameters $\Delta H^{\ddagger}$ and $\Delta S^{\ddagger}$ were calculated, and the value of k_α was extrapolated to 25 °C (Table 1). This switch from $H_2PO_4^-$ (with **2d)** to H_3PO_4 (with **2e**) as the demetalating species is quite remarkable.

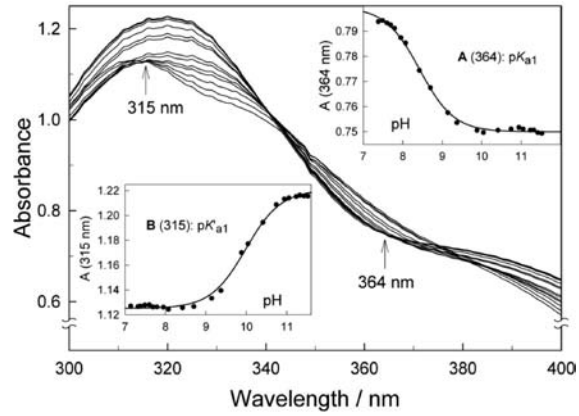

Figure 4. Spectral variations of **2e** (5×10^{-5} M) in the pH range 7.1−11.5. Insets A and B show the spectral changes at 364 and 315 nm, respectively, selected for calculating pK_{a1} and pK'_{a1}. Solid lines in the insets are calculated using the best-fit parameters of eq 2. See text for details.

The data for k_α in Table 1 show that the values of k_α for $H_2PO_4^-$ and complexes **1a** and **2e** are close and **1a** is even slightly more resistant to the demetalation by $H_2PO_4^-$. The enthalpies and entropies of activation, $\Delta H^{\ddagger}$ and $\Delta S^{\ddagger}$ are also similar (Table 1). These similarities suggest that **1** and **2** adopt similar reaction mechanisms. Large and negative enthalpies of activation are consistent with an ordered transition state. Thus, the model of "coordinative" proton delivery by a general acid at the Fe−N bond of the Fe^{III}−TAML in the rate-limiting step as previously proposed[13] is fully consistent with the data reported here. However, because **2d** is less stable in buffered aqueous solutions, **2e** became the focus of more detailed studies.

pH Titration of 2e: Evidence for Octahedral Coordination in Water. Solid Fe^{III}−TAMLs are five-coordinated square-pyramidal species as in Figure 1.[5] In water, they become octahedral with two axial aqua ligands.[26] The pK_a values for the deprotonation of the first coordinated water in **1** fall in the range of 9.3−10.5.[10,11,26] Since these values determine the catalytic oxidation activity of the **1** Fe^{III}−TAMLs,[5] the spectrophotometric pH titration of **2e** was carried out. The deprotonation of **1** induces large changes in the UV/vis spectrum. The spectrum of **2e** is less sensitive to the pH variation in the range of 7.1−11.5 (Figure 4). But unlike with the **1** catalysts, there are no clear-cut isosbestic points over the entire pH range, though the absorbance is pH invariant at 315 and 364 nm at lower and higher pH values, respectively. The changes in absorbance at these two wavelengths are shown in Figure 4 in insets B and A, respectively. Spectral variations in each correspond to a typical acid−base equilibrium involving one proton. Therefore, we conclude that both axial aqua ligands of the octahedral species **2e** in water undergo deprotonation in this pH range as shown in the boxed part of Scheme 2.

We propose that the wavelengths of 315 and 364 nm correspond to the isosbestic points for the first (K_{a1}) and the second (K'_{a1}) equilibria, respectively. The spectral changes at

(26) Ghosh, A.; Ryabov, A. D.; Mayer, S. M.; Horner, D. C.; Prasuhn, D. E., Jr.; Sen Gupta, S.; Vuocolo, L.; Culver, C.; Hendrich, M. P.; Rickard, C. E. F.; Norman, R. E.; Horwitz, C. P.; Collins, T. J. *J. Am. Chem. Soc.* **2003**, *125*, 12378–12378.
(27) Smith, R. M.; Martell, A. E. *Critical Stability Constants*; Plenum Press: New York, 1976; Vol. 4.

Scheme 2. Acid−base Equilibria Involving **2e** (in the Box) and Hydrogen Peroxide to Produce Species That React Pairwise To Afford Oxidized TAML (See Scheme 3)[a]

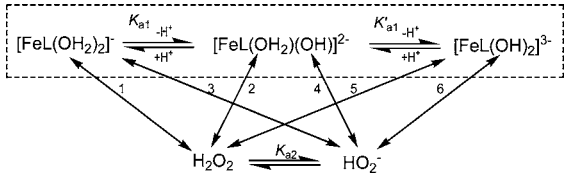

[a] Numerals at the two-sided arrows 1−6 correspond to the rate constants k_1−k_6, respectively.

these wavelengths can be used for a separate evaluation of the K'_{a1} and K_{a1} values, respectively. The data shown in insets **A** and **B** to Figure 4 were fitted to eq 2 (ε_1 and ε_2 are the extinction coefficients for the protonated and deprotonated forms, respectively; see the Supporting Information).

$$\frac{A}{[Fe^{III}]_t} = \frac{\varepsilon_1[H^+] + \varepsilon_2 K_a}{[H^+] + K_a} \quad (2)$$

The values of pK_{a1} and pK'_{a1} thus obtained equal 8.4 ± 0.1 and 10.0 ± 0.1, respectively. The former is the lowest pK_a value observed for any Fe^{III}−TAML investigated to date, suggesting that **2e** has the highest effective positive charge at iron. Achieving this low pK_{a1} of 8.4 has been a long-term goal of the Fe^{III}−TAML design program because the most rapidly reacting species with H_2O_2, the dianion $[FeL(OH_2)(OH)]^{2-}$,[10] can now be generated at a pH that lies closer to 7 and within the pH regime of environmental and even drinking waters. The value of the second pK'_{a1} of 10.0 represents the first case where a second pK_a has been measured because it occurs at a low enough pH to be distinctively observed. The protonation/deprotonation impacts the charge and aggressiveness of the catalytic intermediates in industrially significant mildly basic pH region. It therefore provides a possible way to alter selectivity over a rather narrow pH range.

Moving the Peak of Catalytic Activity to Neutral pH. Mechanistically, Fe^{III}−TAMLs are functional replicas of peroxidase enzymes adopting the minimalistic mechanism of catalysis shown in Scheme 3.[5,10] This mechanism is consistent with eq 3, which becomes eq 4 because k_{-I} is usually negligible.

$$\frac{\text{rate}}{[Fe^{III}\text{−TAML}]_t} = \frac{k_I k_{II}[H_2O_2][S]}{k_{-I} + k_I[H_2O_2] + k_{II}[S]} \quad (3)$$

$$\frac{\text{rate}}{[Fe^{III}\text{−TAML}]_t} = \frac{k_I k_{II}[H_2O_2][S]}{k_I[H_2O_2] + k_{II}[S]} \quad (4)$$

As with the majority of artificial low-molecular weight catalysts for activation of H_2O_2,[10] the relation $k_I[H_2O_2] < k_{II}[S]$ holds for Fe^{III}−TAMLs such that the activation of H_2O_2 is usually the rate-limiting step. Therefore, to achieve more effective catalysts, the k_I step should be positively impacted by design changes in the macrocycle. Our previous studies[5,10] have demonstrated that among the Fe^{III}−TAML species coexisting in water, the most reactive is $[FeL(OH_2)(OH)]^{2+}$ (Scheme 2),

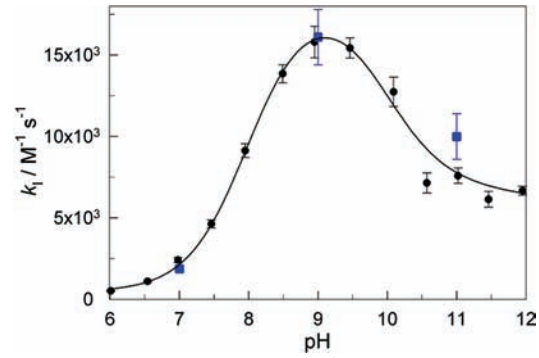

Figure 5. Rate constants k_I calculated using *i* routine as a function of pH for activation of H_2O_2 by **2e** (circles). Blue squares show data obtained previously from 3D regressions.[14] The solid line is calculated using the best-fit parameters of eq 5. See text for details.

making any acquired ability to alter the value of pK_{a1} into a tool for deliberately increasing or decreasing the catalytic reactivity with pH.[11] This explains why the lowest value of pK_{a1}, described here for **2e**, promised higher values of k_I at neutral pH for **2e**. Therefore in order to build up detailed pH profiles for k_I and k_{II}, we investigated the initial rate of Orange II bleaching as a function of $[H_2O_2]$ concentration in the range of 0.0003−0.0015 M at [Orange II] = 4×10^{-5} M in the pH range of 6−12. The hyperbolic dependencies of the rate vs $[H_2O_2]$ were analyzed in terms of eq 4 using four different routines: (i) by calculating the slope of a linear portion of the rate vs $[H_2O_2]$ plot at lower peroxide concentrations, which corresponds to k_I, (ii) by fitting the experimental data to eq 4 using the nonlinear least-squares, and by linearizing the experimental data using the Lineweaver−Burk (iii) and Eadie−Hofstee (iv) routines.[28] In all four cases, consistent values of k_I and k_{II} were obtained, revealing the highest values for both rate constants at pH around 9 (Figure 5 and Figure 2S, Supporting Information). However, it should be mentioned that the Lineweaver−Burk and the Eadie−Hofstee routines provide higher values for k_I by a factor of 1.5−1.7. The rate constants k_I obtained using routine *i* were the closest to those determined previously at pH 7, 9, and 11 from the 3D plots with many more data points,[14] and therefore, this particular set of data shown in Figure 4 was further used for the quantitative analysis. The data in Figure 5 demonstrate that **2e** shows remarkable activity at pH 7.5−8.0 in terms of k_I. This is of exceptional practical value because the rate constants k_{II} for Fe^{III}−TAMLs (and other artificial activators of peroxides) are usually larger than k_I such that the latter controls the process time in water purification applications.[5] The rule holds for **2e** in the studies described here (Figure 2S).

The pH profiles for k_I in the range of 6−12 for Fe^{III}−TAMLs of the first generation, such as in Figure 5, were rationalized in terms of Scheme 2 neglecting the second ionization of an aqua ligand of the **1** catalysts driven by K'_{a1}[10] because this event was not observed at pH below 12. However, it must be taken into consideration for the **2** catalysts. This implies that six parallel pathways with the rate constants k_1−k_6 may contribute the overall k_I pathway. Therefore, the expression for k_I appears as eq 5 with the pathways k_2 and k_3 as well as k_4 and k_5 being kinetically indistinguishable.

Scheme 3. General Mechanism of Catalysis by Fe^{III}−TAML Activators of Peroxides

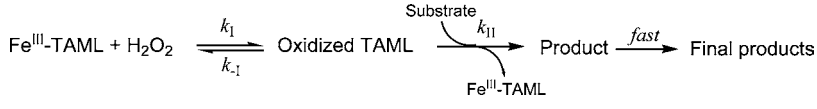

$$k_I = \frac{k_1[H^+]^3 + (k_2K_{a1} + k_3K_{a2})[H^+]^2 + (k_4K_{a1}K_{a2} + k_5K_{a1}K'_{a1})[H^+] + k_6K_{a1}K_{a2}K'_{a1}}{[H^+]^3 + (K_{a1} + K_{a2})[H^+]^2 + (K_{a1}K_{a2} + K_{a1}K'_{a1})[H^+] + K_{a1}K_{a2}K'_{a1}} \quad (5)$$

There is no doubt that eq 5 with cubic terms in $[H^+]$ could be used to fit the data in Figure 4 because such asymmetric bell-shaped plots can be satisfactorily fitted using similar equations with just square terms in $[H^+]$.[10,11] This creates the concern that the calculated rate constants might not represent unique solutions. However, the three K_a values in eq 5 have been experimentally determined independently. Thus, confidence in the calculated rate constants can be increased if the best fit K_a's are close in value to the experimental numbers as reported below. Fitting of the data in Figure 5 to eq 5 was performed by allowing all variables to float as combined terms; i.e., the data were fitted to the equation $(a_1x^3 + a_2x^2 + a_3x + a_4)/(x^3 + b_1x^2 + b_2x + b_3)$. Then, the individual equilibrium constants were obtained by solving a system of three equations consisting of the three b_i terms of the denominator. Those values were further used to calculate rate constants k_1-k_6 from the values of a_i. It should be noted that for the kinetically indistinguishable pathways (k_2 or k_3, and k_3 or k_4), the rate constants were calculated by assuming that the corresponding counterpart equals zero. The thus-derived best-fit values for the equilibrium and the rate constants ($M^{-1}\,s^{-1}$) are as follows: $pK_{a1} = 8 \pm 1$, $pK'_{a1} = 10 \pm 1$, $pK_{a2} = 11.8 \pm 0.9$, $k_1 = (5 \pm 5) \times 10^2$, $k_2 = (2.0 \pm 0.4) \times 10^4$, $k_3 \approx 1.2 \times 10^8$, $k_4 > 4.8 \times 10^5$, $k_5 = (7.6 \pm 1.7) \times 10^3$, and $k_6 \approx 6.2 \times 10^2$. Importantly, there is a good agreement between the values of pK_{a1} and pK'_{a1} measured spectrophotometrically by the UV/vis titration of **2e** (Figure 4) and obtained by fitting the kinetic data. The pK_{a2} value for H_2O_2 (11.8) also agrees reasonably well with those reported in the literature (11.2−11.6).[29] Note again that the rate constants for the kinetically indistinguishable pathways were estimated on the assumption that the corresponding counterpart is negligible, thus making the reported values of k_2-k_5 upper limits. While the calculated rate constants k_1-k_6 are high, it is worth noting that k_3 is the largest. It exceeds the rate constant for formation of compound I from resting state horseradish peroxidase and H_2O_2 under optimal conditions (1.2×10^7 $M^{-1}\,s^{-1}$).[30]

Assessing the Potential for Endocrine Disrupting Activity. Finally, because all chemists must learn how to preempt endocrine disruption in chemical products and processes in accordance with green chemistry principles, we began an exploration for possible endocrine disrupting activity by examining whether **1a**,**b** or **2e** activate transcription mediated by the human thyroid receptor (TRβ), human estrogen receptor (ERα), and rat androgen receptor (AR). The data in Figure 6 were obtained over a concentration range for each Fe^{III}−TAML that include process conditions (1×10^{-8} to 1×10^{-5} M) and anticipated values for environmental receiving waters (1×10^{-11} to 1×10^{-9} M). The data show that none of the Fe^{III}−TAML compounds induced reporter gene activity above what was observed by water alone, whereas the control ligands for each of the receptors induced reporter gene activity as expected. The results demonstrate that **1a**,**b** and **2e** do not activate transcription mediated by these nuclear hormone receptors, suggesting that they do not bind to the receptors. While endocrine disrupting effects can arise via numerous mechanisms,[31] activation of nuclear hormone receptors, and particularly AR, ER, and TR, is associated with many observed endocrine disruption effects. Thus, the inability of Fe^{III}−TAML to activate these receptors is an important finding.

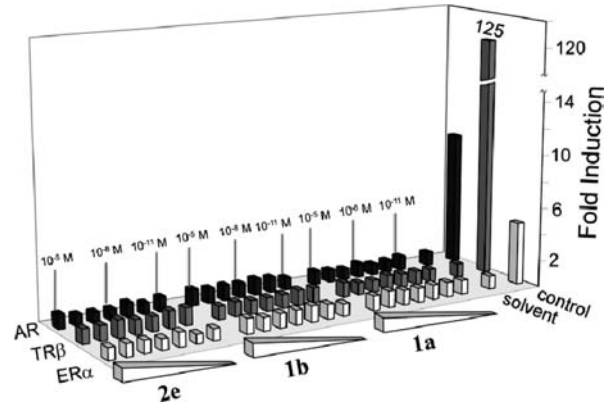

Figure 6. Activation studies showing that Fe^{III}−TAMLs do not activate the nuclear hormone receptors, human TRβ, human ERα, and rat AR. The abilities of solvent (H_2O), control ligands [TRβ (triiodothyronine, 10 nM), ERα (17-β-estradiol, 10 nM), and AR (dihydrotestosterone, 10 nM)] and Fe^{III}−TAMLs, **1a**, **1b**, and **2e** (1×10^{-5} M, 1×10^{-6} M, ..., 1×10^{-11} M) to induce receptor-dependent transcription from reporter gene constructs were tested in transient transfection assays. The data presented are based on three independent experiments, each performed in triplicate ($N = 9$) (see the Supporting Information).

In conclusion, this study shows that mechanistically monitored green oxidation catalyst design, focusing on fundamental properties such as the pK_a's of the catalyst's aqua ligands, can be used to shift the pH-dependent reactivity profile such that the maximum reactivity moves nearer to the pH region of environmental waters where there is a pressing need for improved water purification technologies. Fe^{III}−TAMLs of the second generation (**2**) have acquired much higher peroxide activation reactivity in the pH range of 7.5−8.0 than their **1** progenitors. In addition, catalysts **2d** and **2e** represent a design evolution that has succeeded in bringing about an active species changeover in the demetalation chemistry−while **2d** is destroyed by $H_2PO_4^-$, the much stronger acid H_3PO_4 is needed to eject iron from **2e** at a similar rate. Kinetic studies of **2e**-catalyzed H_2O_2 bleaching of Orange II indicate the catalyst is the optimal peroxidase replica to date in terms of the speed of peroxide activation (k_I) and further oxidation of the test dye (k_{II}) making it all the more promising for use in the oxidative purification of contaminated waters.

This study also highlights what is nothing less than an ethical imperative for not only green but all chemists. Prior to commercial development, at best available standards, any new green chemical product or process should not contain or lead to an endocrine disruptor, or if the benefit is so great that ED activity must be accepted, there should be a strategy in place for mitigating the environmental consequences. To this end, we have taken initial steps toward exhibiting the kind of collabora-

(28) Fersht, A. *Structure and Mechanism in Protein Science: A Guide to Enzyme Catalysis and Protein Folding*: Freeman: New York, 1999.
(29) Jones, C. W. *Applications of Hydrogen Peroxide and Derivatives*; The Royal Society of Chemistry: Cambridge, 1999.
(30) Dunford, H. B. *Heme Peroxidases*. Wiley-VCH: New York, 1999.
(31) Gore, A. C., *Endocrine-Disrupting Chemicals: From Basic Research to Clinical Practice*; Humana Press, Inc.: Totowa, NJ, 2007.

tion that will be needed to evaluate the endocrine disrupting potential of the **2** catalysts. Assays of the type presented here, in combination with others under development, should become routine analytical procedures, just as with elemental analysis and appropriate spectroscopic characterization, as a practical component of honoring Paul Anastas' definition of green chemistry as "the design chemical products and processes that reduce or eliminate the use and generation of hazardous substances".[32]

Acknowledgment. Support is acknowledged from the Heinz Endowments (T.J.C), the Charles E. Kaufman Foundation (T.J.C.), the R.K. Mellon Foundation (W.C.E.), the National Institutes of Environmental Health Sciences (B.B., 5R01-ES015849), the Norwegian Research Council (Miljø 2015: 181888), and the Howard Hughes Medical Institute for support of undergraduate researchers (C.T.T. and R.R.). We thank Roberto Gil for assistance with NMR and the NSF for NMR Instrumentation (CHE-0130903).

Note Added after ASAP Publication. The version published ASAP June 21, 2010 had errors in equations 3 and 4. The corrected version published June 25, 2010.

Supporting Information Available: Scheme 1S; crystal structure data for **2f**; the Eyring plot for the rate constants k_α for in interaction between **2e** and $H_2PO_4^-$; table with the extinction coefficients and K_a for **2e**; pH profiles for the rate constants k_I and k_{II} calculated using the Eadie−Hofstee and Lineweaver−Burke routines for the **2e**-catalyzed oxidation of Orange II; and raw data for luciferase assays. This material is available free of charge via the Internet at http://pubs.acs.org.

JA102524V

(32) EPA website: http://www.epa.gov/greenchemistry.